Journal of
Mechanics of
Materials and Structures

DELAMINATION OF THIN COATINGS AT SCRATCHING: EXPERIMENTS AND NUMERICS

Fredrik Wredenberg and Per-Lennart Larsson

Volume 4, Nº 6 June 2009

mathematical sciences publishers

JOURNAL OF MECHANICS OF MATERIALS AND STRUCTURES
Vol. 4, No. 6, 2009

DELAMINATION OF THIN COATINGS AT SCRATCHING: EXPERIMENTS AND NUMERICS

FREDRIK WREDENBERG AND PER-LENNART LARSSON

Scratching of thin coatings on hard substrates is studied experimentally and numerically, in the latter case by use of the finite element method. In particular the delamination behaviour at scratching, by increasing the normal load up to failure, is of interest. The adhesion of the coating to the substrate is modelled as a cohesive zone where relevant model parameters are determined experimentally using the double cantilever beam test with uneven bending moments (DCB-UBM). Good correlation between experimental and numerical results were achieved and the most important finding confirms the fact that the delamination behaviour was very much dependent on the critical energy release rate of the film/substrate interface. The results achieved are directly relevant for thin film polymer coatings but can also be applied in more general situations as a comprehensive parameter study is performed using the finite element method.

1. Introduction

Scratch testing is commonly used as a technique for studying mechanical properties of materials near their surface. In one of the earliest attempts to use scratching for characterisation, Mohs introduced his hardness scale [1824], in which materials were graded based on the capacity of a harder material to leave a visible scratch on a softer material if the two are rubbed against each other. The scratch test may also be used to test the adhesion of coatings, as is done throughout the coating industry. Typically then, a diamond stylus is drawn across a coated surface with increasing normal load until some well defined failure occurs and the critical load is achieved. This technique can be of substantial importance and is used for the ranking of coating adhesion. Furthermore the scratch test is used for tribological testing.

It is possible to distinguish between two main different types of scratching mechanism. The first one, which here is termed *mild* scratching, is when the behaviour does not involve or is not significantly influenced by any interface properties. If the material is sufficiently tough the scratch deformation will be governed by the bulk constitutive properties. The second type, termed *severe* scratching, occurs if the material toughness is sufficiently low and the formation of cracks takes place. Alternatively, when scratching of coatings is at issue, delamination occurs. Regarding the transition from mild to severe scratching, experimental results are presented in [Bertrand-Lambotte et al. 2002]. It appears likely, at least if no cracks develop, that the scratch process is very similar to conventional indentation testing and that thus can be well described by conventional material properties. In fact, scratch tests have been used to measure elastic and plastic properties [Xie and Hawthorne 2000].

Indentation testing and scratch testing, indeed, show many similar features. When it comes to indentation a great deal of knowledge has been gained over the years regarding the mechanical behaviour at

Keywords: scratching, finite element analysis, contact, delamination, cohesive zone, adhesion, thin film.

indentation. Sharp indenters are most often used, for practical reasons, at least when modern experimental devices such as the nanoindenter (or other types of instrumented indentation devices) are at issue. For such indenters semiempirical relations for material characterisation were derived and used already in the late 1940's and early 1950's, in particular for metals and alloys [Tabor 1951]. In short, from comprehensive experimental investigations Tabor derives a relation

$$H = C\sigma_{\text{repr}}, \tag{1}$$

between the indentation hardness H, here defined as the mean contact pressure at indentation and scratching, and the material yield stress σ_{repr} at a representative value on the accumulated (effective) plastic strain, $\epsilon_{\text{p}} = \epsilon_{\text{repr}}$.

Based partly on these results, further progress was achieved by Johnson [1970; 1985], who showed from theoretical considerations that indentation testing (for example, indentation hardness H) on different materials can be well correlated by using a nondimensional parameter,

$$\Lambda = \frac{E \tan\beta}{(1-\nu^2)\sigma_{\text{repr}}}, \tag{2}$$

where E is Young's modulus, ν is Poisson's ratio and β the attack angle as specified in Figure 1. Johnson's work also suggests that indentation properties for various materials will fall into one out of three levels as indicated in Figure 2. In short, these levels can be characterised as follows. In level I, $\Lambda \leq 3$, very little plastic deformation occurs during the indentation test and all global properties can be derived from an elastic analysis. In level II, $3 < \Lambda \leq 30$, an increasing amount of plastic deformation is present and both the elastic and the plastic properties of the material will influence the outcome of a hardness test according to [Johnson 1970; 1985].

Finally, in level III, $\Lambda > 30$, plastic deformation is present all over the contact area and elasticity no longer influences the hardness value of the material. This is also the region pertinent to most standard engineering metals, and it is also the region where the Tabor formula (1) applies. The indentation results presented in [Tabor 1951] and [Johnson 1970; 1985] have in previous years been verified (and also improved) by the use of finite element methods [Laursen and Simo 1992; Giannakopoulos et al. 1994; Laval 1995; Larsson et al. 1996; Mesarovic and Fleck 1999].

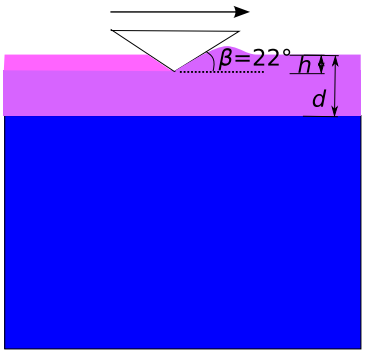

Figure 1. The stylus scratching the film at a depth of h. The film has thickness d and the stylus has attack angle $\beta = 22°$.

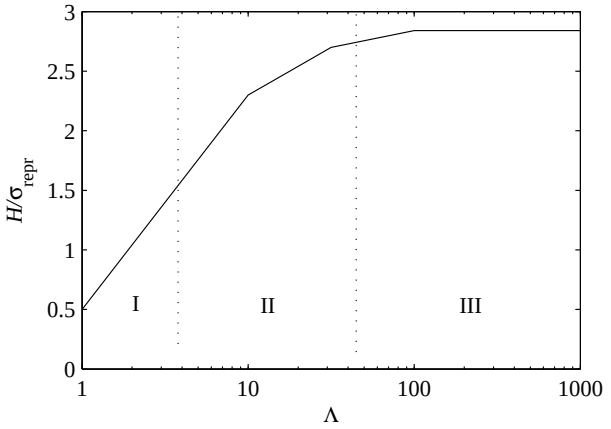

Figure 2. Sketch of the characteristic behaviour of indentation hardness [Johnson 1985]. The indentation hardness H divided by the representative stress σ_{repr} is plotted against the nondimensional strain parameter Λ.

In the same manner as for indentation testing, Bucaille et al. [2001] analyse cone scratching of perfectly plastic materials and their results also indicate that the Johnson parameter in (2) can, indeed, be used for the correlation of scratch parameters as well as indentation parameters. In the same reference the authors find, as could be expected, that the strain levels at scratching are much higher than at indentation, but this finding is not explored in connection with the concept of representative strains (as only perfectly plastic material behaviour is at issue).

Wredenberg and Larsson [2007] present a numerical approach for modelling the scratch test (from a mechanical point of view) using the finite element method. For one thing, these authors find that there exists a representative level of plastic strain of approximately 35% at frictionless scratching using a conical stylus with $\beta = 22°$. The corresponding stress level ($\sigma_{\text{repr}} = \sigma$ when $\epsilon_{\text{p}} = 35\%$) was used throughout our analysis when appropriate. Furthermore, as the scratch test is often used to determine characteristics of polymeric coatings, this is also under investigation [Briscoe et al. 1996; Gauthier et al. 2001]. It should be mentioned in this context that for polymers in particular, the Johnson parameter Λ only gives a rough estimate of the deformation behaviour at scratching due to strain hardening effects in the material surrounding the stylus [Bucaille 2001; Bucaille et al. 2002; Hochstetter et al. 2003; Bucaille et al. 2004]. The representative strain value is of course also dependent on the conical angle and the material law. Due to the complexity of the boundary value problem at scratching, high accuracy of results can only be obtained if numerical methods, preferably the finite element method (FEM), are relied upon. Recently quite a few such analyses have been presented, and further progress based on FEM analyses of the scratch test has also been achieved in [Bucaille et al. 2004] for polymeric materials modelled by using standard elastoplasticity, corresponding to stage II rheology (see Figure 2).

When performing scratch experiments a number of phenomena may complicate the evaluations of the experiments. Estimating the scratch depth can prove arduous due to difficulties in detecting initial contact, at least when using a conical stylus. During scratching of polymeric materials, time dependence may come into effect [Briscoe et al. 1996], both during the actual scratching and afterwards when the

residual deformation is to be measured. Also at scratching of polymers, the deformation is to a great extent elastic, making the estimation of the actual contact area based on the residual groove complicated [Briscoe et al. 1996].

From a practical point of view, a very important aspect of scratching of thin film/substrate systems concerns delamination along the film-substrate interface. This matter has been rather extensively investigated for hard coatings but not so for soft films (perhaps the only exception being results in [Yueguang et al. 2002] pertinent to the "scraping" of a plastic lamella off a substrate). Possible reasons for this are the inherent difficulties associated with an analysis relating the delamination load to the elastic plastic deformation around the stylus. In this context, it was established as far back as [Benjamin and Weaver 1960] that the delamination load primarily depends on the properties of the interface between film and substrate, while Frey et al. [1994], for example, suggest that delamination can be determined by measuring the apparent coefficient of friction.

With all this in mind it seems desirable to perform an investigation of the delamination behaviour at scratching of soft thin films on hard substrates. This was also the aim of this study, where the delamination mechanism of thin polymeric films, undergoing large deformations and high levels of plasticity, was analysed numerically and experimentally. In doing so, when polymeric films are at issue, the deformation of the substrate was neglected for obvious reasons. A previously experimentally characterised vinyl ester plate [Wredenberg and Larsson 2009] was machined to a thin film and adhered to a steel substrate using an epoxy resin. This was done to minimise the residual stresses [Francis et al. 2002] and material property gradients intrinsic to the polymerisation of a film directly to the substrate. Additionally, this enabled testing of the mechanical properties of the film material in bulk, which can be difficult if the film material exists only in a "film state". Furthermore the scratch procedure was simulated numerically using the finite element method. In the simulations the adhesion of the film to the substrate was represented by a cohesive zone. The numerical simulation allowed for the variation of cohesive properties of the film substrate interface as well as for the mechanical properties of the film itself, resulting in a relatively extensive parametric study. The use of a cohesive zone model allows for the definition of a separation energy, G_c, necessary for the delamination of the film, as suggested by many authors for the case of elastic films [Bull 1991; Perry 1983; Malzbender and de With 2001].

We should note that a detailed description of the constitutive behaviour of the polymeric coating was not our highest priority, but rather the investigation of the fracture behaviour of the coating/substrate system.

2. Theoretical background

The present analysis is concerned with the scratching of thin film/substrate systems using a sharp conical stylus assumed to be rigid. It therefore seems appropriate to first of all introduce some basic quantities related to scratching. In the presentation below, F and A represent contact load and contact area, the indices n and t represent the normal and tangential components of these quantities, and h is the scratch depth shown in Figure 1. It should also be mentioned that quasistatic conditions are assumed to prevail during the scratching process.

The hardness quantities of interest during scratching are the normal hardness,

$$H_n = F_n/A_n, \tag{3}$$

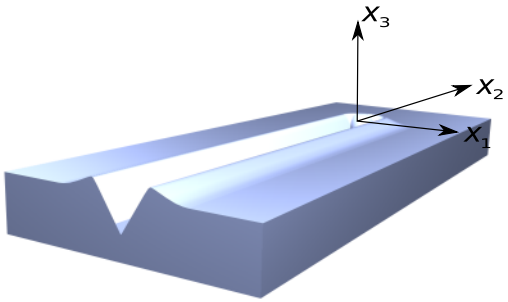

Figure 3. Cartesian coordinates x_i (following the tip of the stylus). Scratching is performed in the x_2 direction.

and the tangential hardness,

$$H_{\mathrm{t}} = F_{\mathrm{t}}/A_{\mathrm{t}}. \tag{4}$$

During a scratch test on homogeneous materials, H_{n}, H_{t}, and the ratio $h/\sqrt{A}$ are constant, and stresses and strains are functions of the dimensionless variables $x_{\mathrm{i}}/\sqrt{A}$ (the Cartesian coordinate system is shown in Figure 3) and material properties alone. This is of course not the case at scratching (or normal indentation) of thin film/substrate systems with increasing load, as the field variables then also depend on the ratio h/d, with d being the film thickness as shown in Figure 1. However, when the indentation depth is held constant during the test, steady-state conditions prevail in the absence of cracking and the global quantities defined above are constant.

Another important parameter at scratching is the apparent coefficient of friction defined as

$$\mu_0 = \frac{F_{\mathrm{t}}}{F_{\mathrm{n}}}. \tag{5}$$

This parameter is also sometimes called the macroscopic coefficient of friction and will be discussed in relevant circumstances below.

In the present analysis, as indicated above, it was assumed that the material was adequately described by classical elastoplasticity. Despite this, the resulting boundary value problem became very much involved (particularly so when a film/substrate boundary was introduced into the problem), and it was necessary to use the finite element method in order to arrive at results of acceptable accuracy. The basic numerical scheme for an analysis of the corresponding homogeneous problem is developed in [Wredenberg and Larsson 2007], with characteristics for a thin films analysis being introduced in [Larsson and Wredenberg 2008]. This scheme was also closely adhered to in the present investigation, but obviously while also accounting for cracking using a cohesive zone model. The most important elements in the numerical approach are discussed in some detail below.

For the constitutive specification, the standard incremental rate-independent Prantl–Reuss equations for classical large deformation von Mises plasticity with isotropic hardening were used and formulated according to

$$\hat{\tau}_{ij} = \frac{E}{(1+\nu)}\left(\delta_{ik}\delta_{jl} + \frac{\nu}{(1-2\nu)}\delta_{ij}\delta kl - \frac{3\tau'_{ij}\tau'_{kl} - (E/(1+\nu))}{2\tau_{\mathrm{e}}^2(\frac{2}{3}K + E/(1+\nu))}\right)D_{kl}. \tag{6}$$

In (6), δ_{ij} is the Kronecker identity tensor, D_{ij} is the rate of deformation, and $\hat{\tau}_{ij}$ is the Jaumann rate of the Kirchhoff stress τ_{ij}. The Kirchhoff stress is related to the Cauchy stress σ_{ij} as $\tau_{ij} = J\sigma_{ij}$, where J is the ratio of volume in the current state to volume in the previous state. Furthermore, τ_{e} and $\hat{\tau}_{ij}$ are the von Mises effective stress and deviatoric stress, respectively. Finally, K is the instantaneous slope of the uniaxial compressive Kirchhoff stress. Note that (6) is only valid at plastic loading when $\tau_e = \tau(\epsilon_{\mathrm{p}})$, the initial yield stress being given by $\tau_{\mathrm{Y}} = \tau(0)$. At elastic loading, or unloading, a hypoelastic formulation of Hooke's law, pertinent to the first part of (6), was relied on. Obviously, within this setting, kinematic hardening effects were not included in the analysis. Such effects can certainly influence the outcome of a scratch test but particularly so during the unloading sequence of the test. In this analysis, the loading part of the scratch test was of primary interest and for this reason, only isotropic hardening was considered.

The novelty of this investigation lies in the analysis of delamination between the film and the substrate. In its simplest form the criterion describing initial crack growth reads

$$G = G_{\mathrm{c}}, \tag{7}$$

where G is the total energy release rate and G_{c} is the critical energy release rate at mode I crack propagation. However, it is well known that the delamination process can be severely influenced by mode mixity, and for this reason the more general criterion

$$G = G_{\mathrm{c}}(\psi), \tag{8}$$

was used, as suggested in [Hutchinson and Suo 1991] for mixed mode crack propagation along a weak plane. This energy may then be allowed to vary depending on the mode of crack growth (mode I, mode II or a combination thereof). The mode mixity may be described by a parameter ψ [Hutchinson and Suo 1991], defined as

$$\psi = \frac{2}{\pi} \arctan \frac{K_{II}}{K_I}. \tag{9}$$

Here K_I and K_{II} are mode I and II stress intensity factors, respectively. In the present study this dependence was investigated through the use of the double cantilever beam (DCB) loaded by uneven bending moments (UBM) as described in [Sørensen and Jacobsen 2003] and [Sørensen et al. 2006]. According to these investigations, the energy release rate may be calculated using the J-integral as

$$G = J = \frac{21(M_1^2 + M_2^2) - 6(M_1 M_2)}{4B^2 H^3 E}(1 - \nu^2), \tag{10}$$

assuming plane deformation and $|M_1| < M_2$ (see Figure 4). In (10), B is the specimen width, H the specimen height, E the elastic modulus, and M_1 and M_2 the applied bending moments (see Figure 4). In this case (9) can also be expressed in terms of the bending moments [Sørensen et al. 2006] acting on the DCB as

$$\psi = \frac{2}{\pi} \arctan\Big(\frac{\sqrt{3}}{2} \frac{M_1 + M_2}{M_1 - M2}\Big), \quad |M_1| < M_2. \tag{11}$$

Figure 4. Double cantilever beam with uneven bending moments.

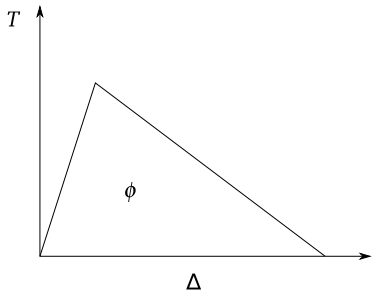

Figure 5. Bilinear traction-separation cohesive law.

The DCB-UBM was chosen since it exhibits the attractive quality of the energy release rate being independent of the crack location, since the crack length is not present in (10); this makes it only necessary to measure the bending moments during the testing.

To be able to model the creation of a new surface with the accompanying separation energy at delamination of a film/substrate interface numerically, a cohesive zone model was used. Commonly the cohesive laws are defined through an interfacial potential ϕ with a traction vector $\boldsymbol{T} = (T_\mathrm{n}, T_\mathrm{t})$ acting on the cohesive surface [Xu and Needleman 1994; Needleman 1987; Ortiz and Pandolfi 1999] as

$$\boldsymbol{T} = \frac{\partial \phi(\boldsymbol{\Delta})}{\partial \boldsymbol{\Delta}}. \tag{12}$$

Here $\boldsymbol{\Delta} = (\Delta_\mathrm{n}, \Delta_\mathrm{t})$ indicates the separation of the surfaces. Generally, as the cohesive surfaces separate the traction will increase until a maximum is reached, after which it will decrease to zero, resulting in complete separation (see Figure 5). Consequently, the area under the curve is the energy needed for separation.

3. Experimental analysis

In conjunction with the scratch experiments, fracture mechanics experiments were conducted to determine the properties of the film/substrate interface. All experiments were performed at room temperature.

3.1. ***The scratch setup.*** Scratching experiments were performed by dragging a conical diamond (with the angle $\beta = 22°$) over the surface of a specimen, using a MTS 66202A-01 biaxial servohydraulic machine with an Instron 8500 control unit. The diamond stylus had a 20 μm tip defect. The normal forces were measured with a MTS load cell and the tangential forces were measured by a load cell built in-house. During the test the normal and tangential forces were recorded. The rotational motion of the actuator was transformed to a translational motion by a carriage sliding on a rail (see Figure 6). During scratching the normal load was linearly increased. After the scratching procedure the specimen was removed and the point of delamination (that is, the position on the specimen where the initial delamination occurred) was recorded and related to the corresponding load. The delamination load was found by measuring the point of initial delamination on the scratched specimen (see Figure 9 on page 1052). As the load was linearly increased during scratching, the delamination load could be found through linear interpolation of the applied scratch load.

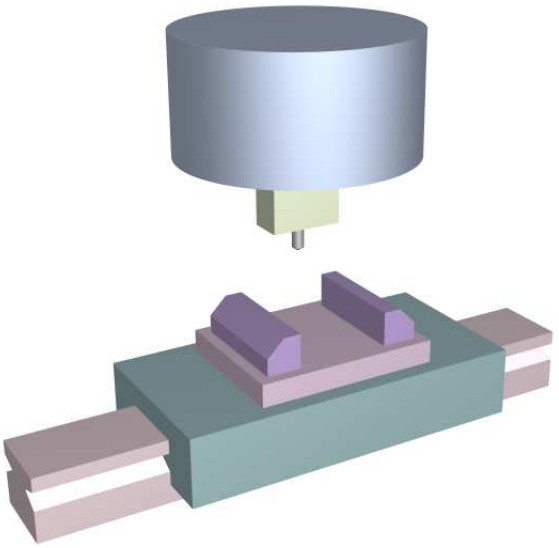

Figure 6. The experimental scratch setup with a carriage (green) sliding on a rail. Above are two force transducers (shear and normal). The specimen is placed in the vice (purple) in the center.

Scratch speeds of 1 mm/s and 0.1 mm/s over a total scratch length of 42 mm were used. The experimental results proved to be somewhat dependent on scratch speed (to be discussed in some detail below). Scratching was initialised at a normal load of 50 N and linearly increased to 150 N during the procedure.

3.2. ***Determination of cohesive parameters.*** In order to determine the mix-mode behaviour of the cohesive law, double cantilever beam specimens were prepared. The specimens were subsequently loaded with uneven bending moments to achieve an arbitrary mode-mixity, ψ [Sørensen et al. 2006], as can be seen in Figure 4. The individual cantilever beams were machined to a length, width B and thickness H of 180 mm, 10 mm and 5 mm, respectively. The contribution of the film strip to the J-integral was assumed to be small as the stiffness of the steel part of the DCB was much larger, and the film strip was thin compared to the steel, thus allowing the energy release rate to be calculated according to (10). As an example, if the contribution of the film strips was taken into account for the case of $M_1 = 0$, this would result in a J approximately 2% larger. The maximum stresses ($\sigma_{\max,\mathrm{n}}$ and $\sigma_{\max,\mathrm{t}}$, to be discussed in some detail below; see Figure 8) in the cohesive law were determined by uniaxial tensile and pure shear tests, where the film was glued between two cylindrical steel bars. The bars were then either pulled apart (tensile) or twisted (shear) with increasing force until the film/steel interface failed. The shear test was set up in the same configuration as the DCB test, with pure bending moments so as to minimise the normal stresses introduced.

3.3. ***Preparation of specimens.*** The scratch specimens were composed of a steel substrate with a vinyl ester film adhered to it by means of an epoxy resin. Prior to adhesion to the substrate, the film was machined to a thickness of 0.9 mm from a thick slate of which bulk mechanical properties have already been investigated in [Wredenberg and Larsson 2009].

After the film was placed on top of the substrate, the specimens were vacuum bagged at 50 kPa and allowed to cure for 24 hours at 40° C. When completed, each specimen was approximately 25 mm wide by 55 mm long and 15 mm thick. The resulting adhesive layer was approximately 6 μm thick.

The DCB specimens were prepared in a similar fashion. Here two steel beams were adhered to a film strip by use of the same epoxy resin as used for the scratch specimen (see Figure 4). To allow for a well defined initial crack, the film strip and the steel beams were given a coat of wax covering the first two centimeters. These specimens were also vacuum bagged and allowed to cure in the same way as in the case of the scratch specimens. Here the resulting adhesive layer was approximately 8 μm thick.

The cylindrical specimens were pushed together by springs (as the shape of the specimen was not suitable for vacuum bagging), giving an adhesive thickness of approximately 5 μm after being cured for 24 hours at 40° C. In all specimens the film thickness was 0.9 mm.

4. Numerical analysis

A numerical analysis using the finite element method was performed with the aid of the commercial FEM package [ABAQUS 2008]. For details of the numerical analysis for homogeneous and film/substrate systems, see [Wredenberg and Larsson 2007; Larsson and Wredenberg 2008]; here we discuss only some basic features and details concerning the cohesive zone analysis. As already stated above, regarding the constitutive specification, the incremental rate-independent Prandtl–Reuss equations for classical large deformation von Mises plasticity with isotropic hardening was relied upon.

As the material experienced very large strains, adaptive meshing was used to maintain the element integrity. The mesh, shown in Figure 7, was composed of some 80000 eight-node linear reduced integration elements. These elements were chosen since they show a faster convergence with respect to mesh refinement than tetrahedral elements and do not have the inherent contact problems of quadratic elements [ABAQUS 2008]. The stylus was assumed to be perfectly rigid and Coulomb friction was assumed when appropriate. All of the results presented are pertinent to a perfectly sharp conical stylus. In order to ensure a relevant comparison between experimental and numerical results, experimental scratch depths were chosen in such a way that any influence from the stylus tip defect was negligible (as investigated carefully in each case through numerical simulations).

As regards boundary conditions, the surface outside the contact area was assumed traction free, and within the area of contact, unilateral kinematic constraints, given by the shape of the conical indenter/stylus depicted in Figure 1, were imposed.

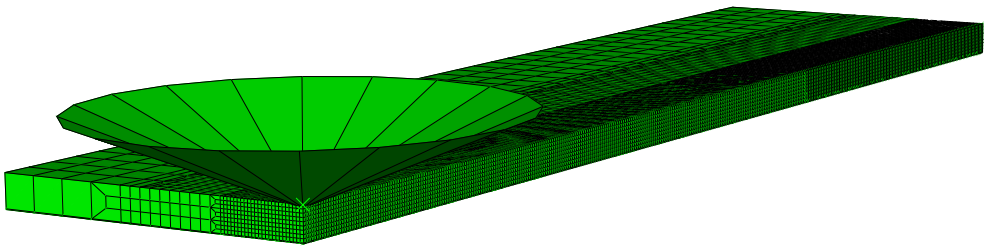

Figure 7. Finite element mesh used in the simulations.

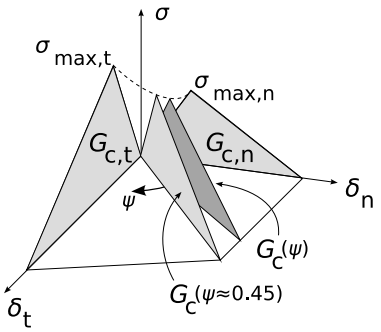

Figure 8. Sketch of the mixed mode cohesive law used in the numerical simulations. The critical energy release rate is labeled $G_c(\psi)$ and the maximum traction σ_{max}. δ indicate crack opening. The indices n and t indicate normal and shear respectively.

To account for the adhesive bond between the film and the substrate, 10000 cohesive elements with a traction-separation law were utilised (see Figure 8). The cohesive law used was defined by five parameters: the maximum cohesive stresses ($\sigma_{max,n}$ and $\sigma_{max,t}$) and the critical energy release rates for three levels of mode-mixity: $G_c(\psi = 0)$, $G_c(\psi \approx 0.45)$ and $G_c(\psi = 1)$. The damage initiation criterion (the dashed line in Figure 8) could be expressed as

$$\left(\frac{\sigma_n}{\sigma_{max,n}}\right)^2 + \left(\frac{\sigma_t}{\sigma_{max,t}}\right)^2 = 1, \tag{13}$$

where σ_n and σ_t are the tractions in the normal and shear direction respectively.

The cohesive elements were for numerical purposes given an initial stiffness (in tension/compression and shear) of 30 TPa/m, corresponding to the initial slope of the cohesive law. A study of the importance of this parameter on the delamination load can be seen in Table 1. From the table it can be concluded that any of the tested stiffness values would suffice. Ultimately the stiffness of 30 TPa/m was chosen as it allows reasonably large elements, and thus lower computational times, as a stiffer cohesive law requires a denser element mesh.

Delamination was said to occur when some cohesive element experienced more than 99% of accumulative damage, meaning that the cohesive deformation had passed the point of maximum traction and that the tractions were down to 99% of the maximum tractions of an undamaged element (see Figure 5). This choice was not of any real importance, but was made in order to avoid any numerical peculiarities involved in the case of a value being 100% accumulated damage. Indeed, changing this value to 100% would cause an indistinguishable change in the simulated delamination load.

Stiffness (TPa/m)	20	30	40	80
Delamination load (N)	87.8	88.6	88.5	87.8

Table 1. Influence of stiffness of the cohesive elements on the delamination load. (The last entry was computed with a higher mesh density.)

5. Results and discussion

Below, the experimental and numerical results in this investigation are shown and analysed. Initially, the relevant experimental results (scratching and cohesive zone results) are presented and discussed. Then, the experimental results are compared with corresponding numerical ones. Such a comparison is certainly of substantial interest in itself but is presently also of interest in order to ensure the reliability of the numerical approach to, in particular, delamination at scratching of thin film/substrate systems. This feature is of direct importance in the present investigation as regards the accuracy of the results of the numerical parametric study included in this study (the presentation of the outcome of the parametric study constitutes the major part of this section of the paper).

5.1. ***Experimental results.*** The normal load at which delamination of the vinyl ester film from the substrate occurred, F_{delam}, can be seen in Table 2, along with the normal scratch hardness H_{n} of (3), at the two different scratch speeds. The hardness was evaluated at half of the scratch length, that is, the scratch width was measured right in the middle between the starting point and finishing point of the residual groove in order to avoid any influence from the specimen boundary. The projected contact area, A_{norm}, was calculated assuming a contact of semicircular shape, according to standard procedure at scratch testing [Williams 1996], as

$$A_{\text{norm}} = (w/2)^2 \frac{\pi}{2}, \tag{14}$$

where w is the residual groove width. The delamination load data did not show a significant dependence on the scratch speed; see Table 2. When averaging all delamination loads regardless of scratch speed the delamination normal load reached the value 105 N (with a standard deviation of 12 N). The corresponding tangential load was found to be 28 N, which was in line with the measured apparent coefficient of friction (μ_0) of 0.28, as will be discussed in some more detail below.

In Figure 9 two typical scratches can be seen along with the delamination of the film (the lighter area). All scratches experienced some cracking in the wake of the stylus as seen in Figure 10. The load at which these cracks formed varied from sample to sample. In around one third of the scratches, delamination occurred prior to the formation of the cracks shown in Figure 10. When investigating this phenomenon, no correlation between the formation of cracks and the delamination load could be found.

As regards the model parameters to be introduced in the numerical analysis, this mainly concerned the constitutive parameters pertinent to the vinyl ester film as well as the interfacial coefficient of friction μ_{i}. The experimentally determined uniaxial stress-strain curve for the vinyl ester film-material is shown in Figure 11. The stress-strain curves in this figure were determined through compression tests of cylindrical specimens, with a length of approximately 5 mm. Some limited sensitivity to strain (deformation) rate effects were found, but as shown in Table 2 the delamination load is not influenced significantly. Again,

Scratch speed (mm/s)	F_{delam} (N)	H_{n} (MPa)
0.1	97.5 (8.3)	367 (20)
1.0	110 (11.1)	365 (10)

Table 2. Experimental results for the delamination load F_{delam} and the normal scratch hardness H_{n} (standard deviation).

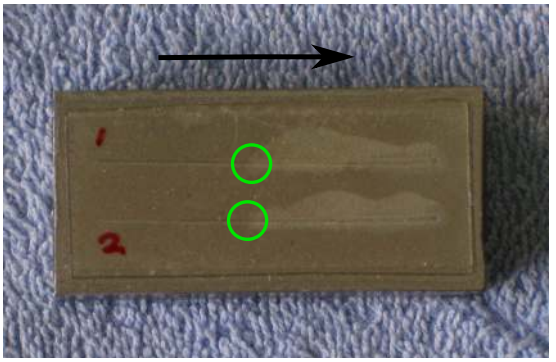

Figure 9. Delaminated scratch specimen with two scratches performed. The points of initial delamination are indicated by green circles. The scratch direction is indicated by the arrow.

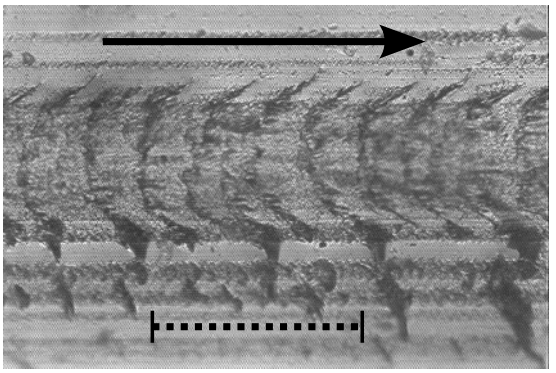

Figure 10. Cracks in the bottom of the scratch groove similar to the ones observed in [Browning et al. 2006; Holmberg et al. 2005]. The scratch direction is indicated by the arrow and the scale is given by the dashed line (0.25 mm). The scratch width was approximately 0.97 mm at this point.

we emphasise that the focus here was the fracture behaviour rather than a detailed description of the constitutive behaviour of the polymer.

Obviously this material exhibits softening after initial plastic deformation. Softening is then followed by extensive hardening, which could not be easily described constitutively as cracking then occurred during the tensile test (as well as barreling during a corresponding compressive test). This issue is discussed below. Furthermore, the uniaxial experiments indicate that the Johnson parameter Λ of (2)) takes on the value 21 for vinyl ester. In [Wredenberg and Larsson 2007; 2009] master curves for the relation between Λ and the ploughing part of the coefficient of friction, here denoted $\mu_{\mathrm{p}}(\Lambda)$, are presented, and it can thus be concluded that $\mu_{\mathrm{p}}(\Lambda) \approx 0.21$ here. The current measurements gave an apparent coefficient of friction of $\mu_0 \approx 0.28$, and remembering that the interfacial and ploughing friction may be separated as

$$\mu_0 = \mu_{\mathrm{i}} + \mu_{\mathrm{p}}(\Lambda), \tag{15}$$

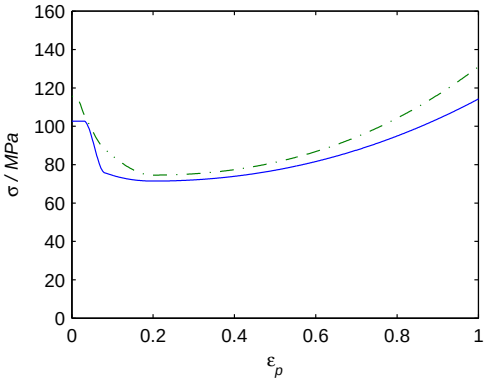

Figure 11. Typical stress-strain curve of the presently analysed vinyl ester. Deformation rates: 0.0001 mm/s (continuous line) and 0.001 mm/s (dotted-dashed line).

for $\mu_{\mathrm{i}} < 0.2$ [Wredenberg and Larsson 2007; Bowden and Tabor 1950; Goddard and Wilman 1962], it was concluded that the coefficient of interfacial friction μ_{i} was 0.07. This value was then used throughout the numerical simulations (in contrast to the situation at normal indentation [Carlsson et al. 2000], relevant local and global variables are quantitatively very much influenced by the presence of interfacial friction).

As regards the fracture mechanics results, double cantilever beam experiments were performed for three different bending moment ratios: $M_1/M_2 = -1$, $M_1/M_2 = 0$ and $M1/M2 = 1$, corresponding to mode mixities $\psi = 0$, $\psi \approx 0.45$ and $\psi = 1$; see (11). As seen in Figure 12, the critical energy release rate is substantially higher for pure mode II ($\psi = 1$) than for pure mode I ($\psi = 0$) loading. The maximum normal cohesive stress and maximum shear cohesive stress were found to be $\sigma_{\max,\mathrm{n}} = 21$ MPa and $\sigma_{\max,\mathrm{t}} = 27$ MPa respectively.

5.2. ***Numerical results: comparison with experiments.*** The numerical model described above was used in the present paper in order to perform a comprehensive parametric study regarding the influence from different parameters on the delamination load. In order to determine the reliability of the numerical approach a comparison between numerical and experimental results pertinent to vinyl ester was performed. Accordingly, corresponding values for delamination load and (normal) scratch hardness were compared. It was then assumed that quasistatic conditions prevailed, that is, that the uniaxial stress-strain relations were determined from experiments performed at such values of the strain rate that rate effects could be

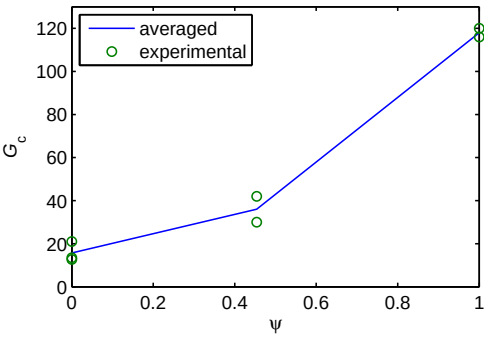

Figure 12. Results from the critical energy release rate measurements.

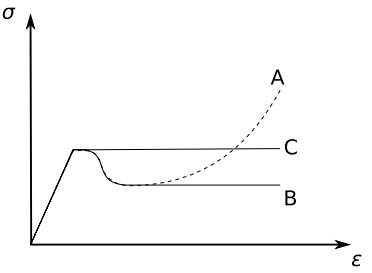

Figure 13. Sketch of film stress-strain relations used in the numerical simulations.

neglected. In this context it should be mentioned that some small rate effects were noticed when the scratch experiments were performed at different speeds; see Table 2. As a comparison at quasistatic conditions were aimed at, the experimental results pertinent to a scratch speed being 0.1 mm/s were used for this purpose.

The shape of the stress-strain curve used in the numerical model deserves some further discussion. As mentioned, the material showed softening after initial deformation and then hardening, as seen in Figures 11 and 13 (material A). This indicates that the value of Λ in (2) is approximately 21. However, as discussed above, the subsequent hardening could not be well described due to cracking (and barreling) during the uniaxial tensile test. For this reason the stress-strain behaviour was modelled, in the numerical simulations, using materials corresponding to curves B and C of Figure 13. Material B is described by no hardening after softening, while material C is an elastic-perfectly plastic material but with the elastic modulus adjusted in such a way that the value of Λ was 21, as determined from the uniaxial experiments.

Remembering that both softening and hardening characterised the material it seems likely that these effects are represented "in average" by material C, and for this reason this material was singled out to be used in the numerical calculations when closeness to experimental conditions was to be investigated. A comparison between experimental and numerical results is shown in Table 3, where it should be emphasised that the hardness values reported correspond to the hardness for a homogeneous vinyl ester material. Obviously, the two sets of results are close and, remembering the difficulties involved in interpreting the outcome of the scratch/delamination experiments, this feature gives some definite confidence in the numerical procedure used in the present analysis, especially considering that qualitative effects are of primary importance to the parametric study (even though quantitative results also are of interest). It should be noted in passing that normal cone indentation of vinyl ester was also performed experimentally and numerically (material C), and that in this case the two sets of results were almost identical, which gives us further confidence in the numerical procedure.

	F_{delam} (N)	H_{n} (MPa)
Experimental	97.5 (8.3)	367 (20)
Simulated	88	344

Table 3. Comparison of simulated and experimental results for the delamination load, F_{delam}, and the normal scratch hardness, H_{n}. (Standard deviation)

Finally in this context it should be emphasised that material C, in Figure 13, was used in the numerical simulations in the present comparison as this material was obviously more appropriate when reproducing the experiments. However, a polymer such as vinyl ester obviously exhibits softening after initial plastic deformation and in order to include this effect in the parametric study presented below it was thought advisable to use material B, in Figure 13, as a reference material in this study. It should be emphasised though that the exclusion of the strain hardening phenomenon renders the results less general.

5.3. ***Numerical results: parametric study.*** In the present parametric study the numerical simulation of scratching of vinyl ester film (material B in Figure 13 in order to include features related to softening) was taken as a reference simulation. Interestingly, in this reference simulation (with the interfacial coefficient of friction being 0.07 as discussed above), the depth at which the delamination occurs is only $h/d \approx 0.16$, which means that the global scratch properties such as friction, hardness etc. are virtually unaffected by the presence of the substrate, according to [Larsson and Wredenberg 2008]. This is of course not the case for systems with tougher interfaces for which the stylus will penetrate further before delamination occurs, but definitely gives some further confidence regarding the assumption of a nondeformable substrate. Indeed a deformable substrate could easily be included in the calculations, but this requires a more comprehensive parametric study, which was not considered in this initial investigation. When appropriate in the presentation below, superscript "sim" and "meas" refer to the parameters used in the simulations and the parameters experimentally determined, respectively. A typical delamination shape is shown in Figure 14.

Initially an investigation of two extremes was made where the cohesive strength (the critical energy release rate G_c and the maximum stress σ_{max}) in either normal or shear mode was set to infinity. As a result it was obvious that the delamination of the vinyl ester film was shear driven, as increasing the cohesive strength in the normal mode had no effect on the delamination load, whereas setting the cohesive strength in the shear mode to infinity led to an "undelaminable" interface.

The numerical study was started with an investigation of the influence from the critical energy release rate. A factor, F_G, defined as

$$G_c^{sim}(\psi) = F_G G_c^{meas}(\psi), \tag{16}$$

was used for this purpose. The results are shown in Figure 15 and it is very obvious that F_G had a strong influence on the delamination load. In all figures concerning the delamination load, legends *normal* and

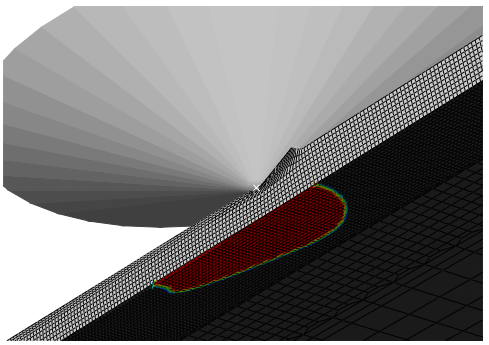

Figure 14. Simulated delamination of a vinyl ester coating (the red area is delaminated).

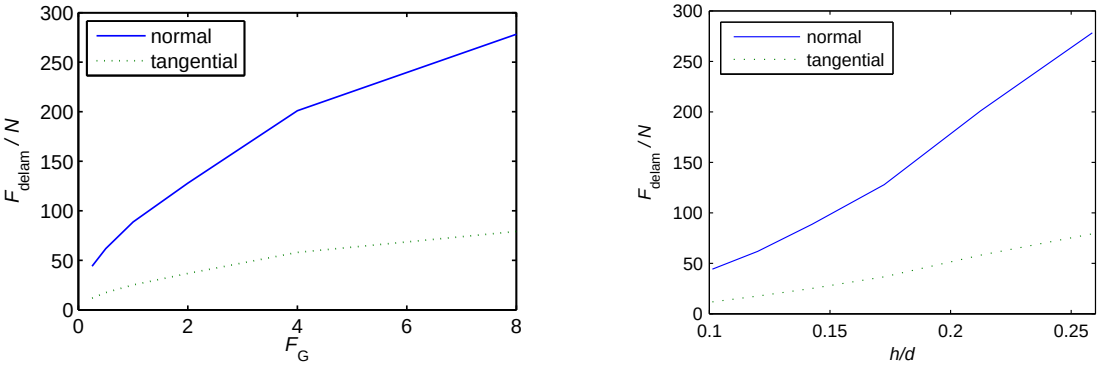

Figure 15. Left: delamination load as a function of the critical energy release rate factor F_G. The maximum cohesive stress is kept constant. Right; delamination load as a function of the scratch depth to coating thickness ratio, h/d.

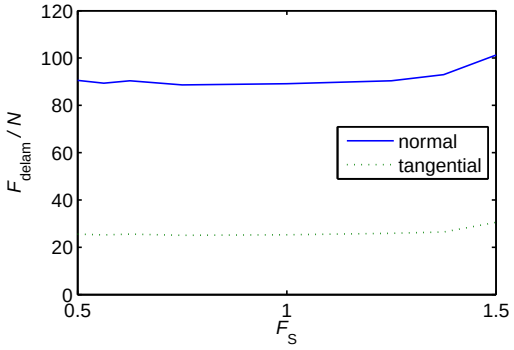

Figure 16. Delamination load as a function of maximum stress factor F_S. The critical energy release rate is kept constant.

tangential refer to the loads acting on the stylus normal to the scratched surface and along the scratched surface in the scratch direction, respectively. In the right half of the figure, the delamination load results from left half are plotted against the scratch depth at delamination to the coating thickness ratio, and the results give further confidence in the assumptions of a nondeformable substrate, as shown in [Larsson and Wredenberg 2008]. Even at the extreme value $h/d \approx 0.25$ substrate effects are very small.

Similarly, we introduced a maximum stress factor F_S, multiplying the maximum cohesive stress ($\sigma_{max,n}$ and $\sigma_{max,t}$) so that

$$\sigma_{max,n}^{sim} = F_S \sigma_{max,n}^{meas}, \tag{17}$$

$$\sigma_{max,t}^{sim} = F_S \sigma_{max,t}^{meas}, \tag{18}$$

while maintaining the same value on the critical energy release rate, in the cohesive law. From the left side of Figure 15 and from Figure 16 it may be concluded that the most influential cohesive parameter, as far as the delamination load is concerned, was the separation energy and to a much lesser extent the maximum cohesive stress.

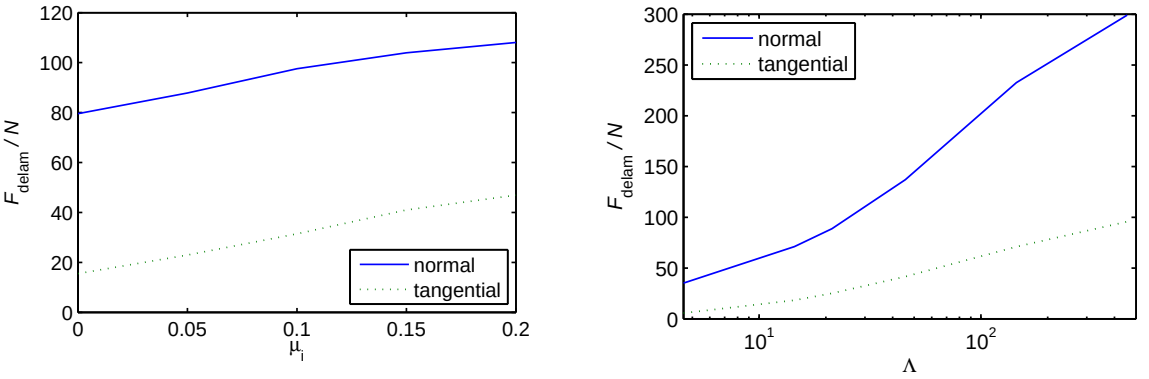

Figure 17. Delamination load as a function of the interfacial coefficient of friction μ_i (left) and of the parameter Λ of (2) (right).

Since the interfacial coefficient of friction μ_i was expected to have a large impact on the delamination load, we performed simulations with varying μ_i (Figure 17, left). For moderate levels of the interfacial coefficient of friction (μ_i), surprisingly little effect on the delamination load was seen, suggesting that frictionless simulations might suffice for most cases. This also indicates that no special regard need be taken to friction when performing scratch experiments in order to determine the adhesion of thin coatings. This certainly simplifies the evaluation of such experiments. As the interfacial friction coefficient μ_i was increased beyond ≈ 0.2 — which was not the case for any of the scratched materials in [Wredenberg and Larsson 2007] — the material in front of the stylus would fold over on itself halting the simulation due to failing mesh integrity, in reality probably causing loss of material.

As in [Wredenberg and Larsson 2007; Larsson and Wredenberg 2008], it may be interesting to relate the delamination load to the Johnson parameter Λ of Equation (2). In Figure 17, right, it can be seen how the delamination force monotonically increases with increasing Λ. This was most likely due to smaller penetration of the stress field into the film layer as the deformation is increasingly dominated by plasticity. Larsson and Wredenberg [2008] find that the global parameters at scratching are more affected by the substrate at low Λ.

Also the ploughing coefficient of friction at the occurrence of delamination showed very similar behaviour to that of homogeneous materials, as reported in [Larsson and Wredenberg 2008]; see Figure 18. In the figure, the ploughing coefficient of friction μ_p was calculated from the results in Figure 17, right, through the use of (15).

Furthermore a yield stress factor, F_P, was defined as

$$\sigma_Y^{\mathrm{sim}} = F_\mathrm{P}\sigma_Y^{\mathrm{meas}}. \tag{19}$$

In (19), σ_Y^{sim} is (with the notation adopted previously) the yield stress used in the simulations and σ_Y^{meas} is the measured yield stress of the vinyl ester. As F_P was varied, the elastic modulus of the film was adjusted in order to maintain the original Λ.

Lowering the yield stress will, as expected also lower the scratch hardness and subsequently increase the scratch depth. On the other hand, increasing the yield stress (as in Figure 19) will increase the hardness of the film and thus keep the region of high stresses away from the film/substrate interface,

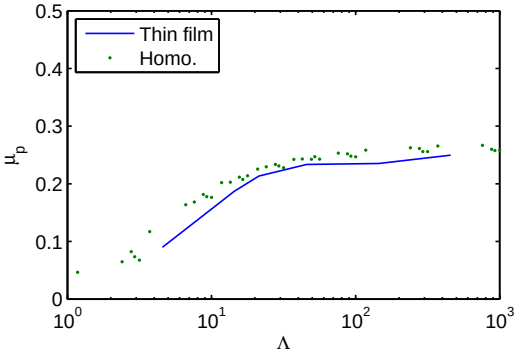

Figure 18. Ploughing coefficient of friction at delamination compared to results for homogeneous materials in [Larsson and Wredenberg 2008].

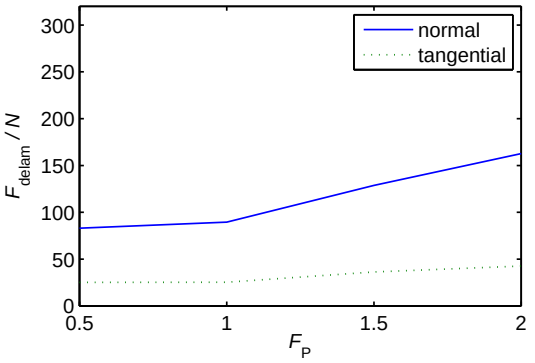

Figure 19. Delamination load as a function of yield stress factor F_P. The Johnson parameter $\Lambda = 21$. For values of $F_P < 0.5$ the film would not delaminate without the stylus actually scraping the substrate.

causing a higher delamination load. When simulating scratching with small values of F_P (< 0.5) the film would not delaminate until the stylus actually scraped the substrate, at which state it may be expected that the stylus tip geometry greatly influenced the outcome of the test.

Since polymeric materials often display pressure sensitivity [Bubeck et al. 1984; Quinson et al. 1997; Rottler and Robbins 2001], this was investigated by means of a Drucker–Prager elastic-plastic material. The pressure sensitivity of a Drucker–Prager material is characterised by (together with the standard assumptions in von Mises plasticity) a parameter known as the *friction angle*, α, allowing the yield stress to vary with the mean stress σ_m. The yield surface (see Figure 20) may then be described as

$$\sigma_e + \tan(\alpha)\sigma_m = \sigma_0, \tag{20}$$

where σ_0 is the yield stress at zero mean stress (pure shear) and σ_e is the effective stress. A series of simulations was performed with different friction angles α.

Figure 21 shows the delamination load as a function of this parameter. Experimentally, for the vinyl ester in question, the friction angle α was found to be very small (about 2°), well within the values tested in Figure 21. This indicates that this phenomenon did not significantly influence the results.

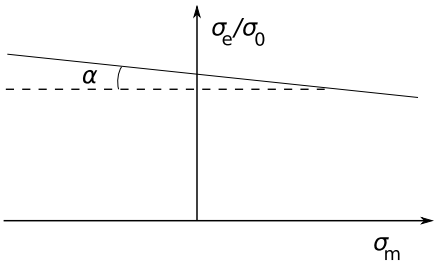

Figure 20. Sketch of the Drucker–Prager yield surface.

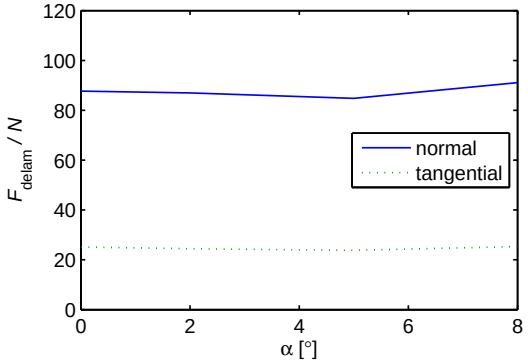

Figure 21. Investigation of the influence of pressure sensitivity (friction angle α) on the delamination load.

As a final comment we stress that the present choice of attack on the delamination problem, using cohesive zone modelling, was based on the fact that such an analysis does not require a preexisting crack. An alternative direct attack on the delamination problem based on linear fracture mechanics, in the spirit of [Nilsson et al. 1993; Larsson 1991], for example, is of course also possible, but less accurate.

6. Conclusions

The present investigation is concerned with experimental and numerical analysis of scratching of thin polymeric films, and particularly with delamination behaviour. The most important results can be summarised as follows:

- The delamination resistance was in large part dependent on the critical energy release rate of the film/substrate interface and less on the maximum tractions of the interface.
- The influence of the coefficient of interfacial friction had only a limited effect on the delamination load.
- Increasing hardness and the Johnson parameter of Equation (2), both important scratch parameters, led to increasing delamination load.
- For moderate levels of pressure sensitivity (such as displayed by the vinyl ester tested in this paper) there was virtually no effect on the delamination load.

Acknowledgements

The authors acknowledge the support of the Swedish Research Council through grant 621-2005-5803. They also thank Prof. Fred Nilsson for valuable advice and discussions, and for reading and commenting on the manuscript; Martin Öberg for his help and advice in the laboratory; and Kurt Lindqvist for manufacturing specimens and experimental equipment.

References

[ABAQUS 2008] *ABAQUS manual*, Version 6.7, Hibbit and Karlsson and Sorensen Inc., Pawtucket, RI, 2008.

[Benjamin and Weaver 1960] P. Benjamin and C. Weaver, "Measurement of adhesion of thin films", *Proc. R. Soc. Lond. A* **254**:1277 (1960), 163–176.

[Bertrand-Lambotte et al. 2002] P. Bertrand-Lambotte, J. L. Loubet, C. Verpy, and S. Pavan, "Understanding of automotive clearcoats scratch resistance", *Thin Solid Films* **420–421** (2002), 281–286.

[Bowden and Tabor 1950] F. P. Bowden and D. Tabor, *The friction and lubrication of solids*, Clarendon, Oxford, 1950.

[Briscoe et al. 1996] B. J. Briscoe, P. D. Evans, S. K. Biswas, and S. K. Sinha, "The hardness of poly(methylmethacrylate)", *Tribol. Int.* **29**:2 (1996), 93–104.

[Browning et al. 2006] R. L. Browning, G.-T. Lim, A. Moyse, H.-J. Sue, H. Chen, and J. D. Earls, "Quantitative evaluation of scratch resistance of polymeric coatings based on a standardized progressive load scratch test", *Surf. Coat. Technol.* **201**:6 (2006), 2970–2976.

[Bubeck et al. 1984] R. A. Bubeck, S. E. Bales, and H.-D. Lee, "Changes in yield and deformation of polycarbonates caused by physical aging", *Polym. Eng. Sci.* **24**:14 (1984), 1142–1148.

[Bucaille 2001] J. L. Bucaille, *Simulation numérique de l'indentation et de la rayure des verres organiques*, Ph.D. thesis, Écoles des Mines de Paris, 2001.

[Bucaille et al. 2001] J. L. Bucaille, E. Felder, and G. Hochstetter, "Mechanical analysis of the scratch test on elastic and perfectly plastic materials with the three-dimensional finite element modeling", *Wear* **249**:5–6 (2001), 422–432.

[Bucaille et al. 2002] J. L. Bucaille, E. Felder, and G. Hochstetter, "Identification of the viscoplastic behavior of a polycarbonate based on experiments and numerical modeling of the nano-indentation test", *J. Mater. Sci.* **37**:18 (2002), 3999–4011.

[Bucaille et al. 2004] J. L. Bucaille, E. Felder, and G. Hochstetter, "Experimental and three-dimensional finite element study of scratch test of polymers at large deformations", *J. Tribol.* (*ASME*) **126**:2 (2004), 372–379.

[Bull 1991] S. J. Bull, "Failure modes in scratch adhesion testing", *Surf. Coat. Technol.* **50**:1 (1991), 25–32.

[Carlsson et al. 2000] S. Carlsson, S. Biwa, and P.-L. Larsson, "On frictional effects at inelastic contact between spherical bodies", *Int. J. Mech. Sci.* **42**:1 (2000), 107–128.

[Francis et al. 2002] L. F. Francis, A. V. McCormick, D. M. Vaessen, and J. A. Payne, "Development and measurement of stress in polymer coatings", *J. Mater. Sci.* **37**:22 (2002), 4717–4731.

[Frey et al. 1994] N. Frey, P. Mettraux, G. Zambelli, and D. Landolt, "Modified scratch test for study of the adhesion of ductile coatings", *Surf. Coat. Technol.* **63**:3 (1994), 167–172.

[Gauthier et al. 2001] C. Gauthier, S. Lafaye, and R. Schirrer, "Elastic recovery of a scratch in a polymeric surface: experiments and analysis", *Tribol. Int.* **34**:7 (2001), 469–479.

[Giannakopoulos et al. 1994] A. E. Giannakopoulos, P.-L. Larsson, and R. Vestergaard, "Analysis of Vickers indentation", *Int. J. Solids Struct.* **31**:19 (1994), 2679–2708.

[Goddard and Wilman 1962] J. Goddard and H. Wilman, "A theory of friction and wear during the abrasion of metals", *Wear* **5**:2 (1962), 114–135.

[Hochstetter et al. 2003] G. Hochstetter, A. Jimenez, J. P. Cano, and E. Felder, "An attempt to determine the true stress-strain curves of amorphous polymers by nanoindentation", *Tribol. Int.* **36**:12 (2003), 973–985.

[Holmberg et al. 2005] K. Holmberg, A. Laukkanen, H. Ronkainen, and K. Wallin, "Tribological analysis of fracture conditions in thin surface coatings by 3D FEM modelling and stress simulations", *Tribol. Int.* **38**:11–12 (2005), 1035–1049.

[Hutchinson and Suo 1991] J. W. Hutchinson and Z. Suo, "Mixed mode cracking in layered materials", *Adv. Appl. Mech.* **29** (1991), 63–191.

[Johnson 1970] K. L. Johnson, "The correlation of indentation experiments", *J. Mech. Phys. Solids* **18**:2 (1970), 115–126.

[Johnson 1985] K. L. Johnson, *Contact mechanics*, Cambridge University Press, Cambridge, 1985.

[Larsson 1991] P.-L. Larsson, "On delamination buckling and growth in circular and annular othotropic plates", *Int. J. Solids Struct.* **27**:1 (1991), 15–28.

[Larsson and Wredenberg 2008] P.-L. Larsson and F. Wredenberg, "On indentation and scratching of thin films on hard substrates", *J. Phys. D Appl. Phys.* **41**:7 (2008), 074022.

[Larsson et al. 1996] P.-L. Larsson, A. E. Giannakopoulos, E. Söderlund, D. J. Rowcliffe, and R. Vestergaard, "Analysis of Berkovich indentation", *Int. J. Solids Struct.* **33**:2 (1996), 221–248.

[Laursen and Simo 1992] T. A. Laursen and J. C. Simo, "A study of the mechanics of microindentation using finite elements", *J. Mater. Res.* **7**:3 (1992), 618–626.

[Laval 1995] P. Laval, *Étude théorique et expérimentale de l'indentation des matériaux élastoplastiques homogènes ou revêtus*, Ph.D. thesis, Écoles des Mines de Paris, 1995.

[Malzbender and de With 2001] J. Malzbender and G. de With, "Analysis of scratch testing of organic-inorganic coatings on glass", *Thin Solid Films* **386**:1 (2001), 68–78.

[Mesarovic and Fleck 1999] S. D. Mesarovic and N. A. Fleck, "Spherical indentation of elastic-plastic solids", *Proc. R. Soc. Lond. A* **455**:1987 (1999), 2707–2728.

[Mohs 1824] F. Mohs, *Grundriss der Mineralogie*, Dresden, 1824.

[Needleman 1987] A. Needleman, "A continuum model for void nucleation by inclusion debonding", *J. Appl. Mech.* (*ASME*) **54**:3 (1987), 523–531.

[Nilsson et al. 1993] K.-F. Nilsson, J. C. Thesken, P. Sindelar, A. E. Giannakopoulos, and B. Storåkers, "A theoretical and experimental investigation of buckling induced delamination growth", *J. Mech. Phys. Solids* **41**:4 (1993), 749–782.

[Ortiz and Pandolfi 1999] M. Ortiz and A. Pandolfi, "Finite-deformation irreversible cohesive elements for three-dimensional crack-propagation analysis", *Int. J. Numer. Methods Eng.* **44**:9 (1999), 1267–1282.

[Perry 1983] A. J. Perry, "Scratch adhesion testing of hard coatings", *Thin Solid Films* **107**:2 (1983), 167–180.

[Quinson et al. 1997] R. Quinson, J. Perez, M. Rink, and A. Pavan, "Yield criteria for amorphous glassy polymers", *J. Mater. Sci.* **32**:5 (1997), 1371–1379.

[Rottler and Robbins 2001] J. Rottler and M. O. Robbins, "Yield conditions for deformation of amorphous polymer glasses", *Phys. Rev. E* **64**:5 (2001), 051801.

[Sørensen and Jacobsen 2003] B. F. Sørensen and T. K. Jacobsen, "Determination of cohesive laws by the *J* integral approach", *Eng. Fract. Mech.* **70**:14 (2003), 1841–1858.

[Sørensen et al. 2006] B. F. Sørensen, K. Jørgensen, T. K. Jacobsen, and R. C. Østergaard, "DCB-specimen loaded with uneven bending moments", *Int. J. Fract.* **141**:1–2 (2006), 163–176.

[Tabor 1951] D. Tabor, *Hardness of metals*, Clarendon, Oxford, 1951.

[Williams 1996] J. A. Williams, "Analytical models of scratch hardness", *Tribol. Int.* **29**:8 (1996), 675–694.

[Wredenberg and Larsson 2007] F. Wredenberg and P.-L. Larsson, "On the numerics and correlation of scratch testing", *J. Mech. Mater. Struct.* **2**:3 (2007), 573–594.

[Wredenberg and Larsson 2009] F. Wredenberg and P.-L. Larsson, "Scratch testing of metals and polymers: experiments and numerics", *Wear* **266**:1–2 (2009), 76–83.

[Xie and Hawthorne 2000] Y. Xie and H. M. Hawthorne, "A controlled scratch test for measuring the elastic property, yield stress and contact stress-strain relationship of a surface", *Surf. Coat. Technol.* **127**:2–3 (2000), 130–137.

[Xu and Needleman 1994] X.-P. Xu and A. Needleman, "Numerical simulations of fast crack growth in brittle solids", *J. Mech. Phys. Solids* **42**:9 (1994), 1397–1434.

[Yueguang et al. 2002] W. Yueguang, Z. Manhong, and T. Shan, "Characterization of the fracture work for ductile film undergoing the micro-scratch", *Acta Mech. Sinica* **18**:5 (2002), 494–505.

Received 4 Nov 2008. Revised 12 Mar 2009. Accepted 2 Jun 2009.

FREDRIK WREDENBERG: fredrik@hallf.kth.se
KTH Solid Mechanics, Royal Institute of Technology, 10044 Stockholm, Sweden

PER-LENNART LARSSON: pelle@hallf.kth.se
KTH Solid Mechanics, Royal Institute of Technology, 10044 Stockholm, Sweden